Cracks and degradation layers in large flat-on-flat fretting contact with steels and cast iron

Janne Juoksukangas[1*], Verner Nurmi[1], Jouko Hintikka[4,1], Mari Honkanen[3], Minnamari Vippola[2,3], Arto Lehtovaara[1], Antti Mäntylä[4], Joona Vaara[4], Tero Frondelius[4,5]

[1]Tribology and Machine Elements, Faculty of Engineering and Natural Sciences, Tampere University, P.O. Box 589, FI-33014 Tampere University, Finland

[2]Materials Characterization, Faculty of Engineering and Natural Sciences, Tampere University, P.O. Box 589, 33014 Tampere University, Finland

[3]Tampere Microscopy Center, Tampere University, P.O. Box 692, FI-33014 Tampere University, Finland

[4]R&D and Engineering, Wärtsilä, P.O.Box 244, 65101 Vaasa, Finland

[5]University of Oulu, Erkki Koiso-Kanttilan katu 1, 90014, Oulu, Finland

*Corresponding author, janne.juoksukangas@tuni.fi, +358408490559

ABSTRACT

Fretting may deteriorate contacts in terms of wear and cracking. Fretting-induced material degradation and frictional behaviour was studied experimentally in a large flat-on-flat fretting contact with a moderate nominal normal pressure and in different sliding conditions. The materials studied were cast iron, structural steel, and quenched and tempered steel. The results for all materials revealed a severely deformed microstructure, a tribologically transformed structure with high hardness, an oxidized third body layer and cracking. The initial peak in the coefficient of friction followed by stabilization occurred in all material pairs in gross sliding conditions. With low utilization of friction, only a limited amount of damage occurred. The results for each of these materials were compared.
Keywords: fretting; friction; cracks; microscopy

1. INTRODUCTION

Fretting can severely damage contact surfaces in terms of wear (fretting wear) and cracking (fretting fatigue) [1]. Fretting is characterized by relative sliding between contacting surfaces, leading to surface degradation. As cracks are created inside contacts, fretting can lead to sudden and serious failure. The magnitude of the oscillating slip is mostly in the range of a few micrometers to some tens or hundreds of micrometers. Damage can occur even when only a portion of the apparent contact area is slipping and the rest is stuck; this is called the partial slip condition. The entire nominal contact

area is sliding in gross sliding conditions. Both these regimes are experienced within the loading history in the mixed slip regime.

The coefficient of friction (hereafter '*COF*') may increase initially up to around 1.5 in gross sliding fretting contacts with steels [2,3]. This leads to high tangential tractions and stresses that can cause fretting fatigue crack nucleation. In addition, the *COF* is seldom constant during loading; rather it increases and may peak at the beginning and stabilize after some tens of thousands of loading cycles [2,4]. There are many non-idealities in fretting contacts, such as non-Coulomb friction, abnormal wear (non-Archard) and adhesion spot induced stress concentrations. Due to these non-idealities [5], the design of machine components can be challenging [6,7]. Contact edges [8,9], the boundary between stick and slip regimes [10] or cold welded junctions [11] are typical locations for crack nucleation in fretting contacts. Fretting-induced cracks tend first to propagate under combined contact and bulk loadings, and beyond the influence of contact loading, cracks continue to grow solely due to cyclic bulk loading [12]. Under the contact shear loading, cracks typically grow at an oblique angle to the contact surface even when the bulk loading is in a parallel direction. Regions suffering severe plastic deformation and cracks at the boundaries of that work hardened region have been observed to occur very early in the loading history, even within hundreds of loading cycles [13].

The existence of tribologically transformed structures (TTS) in tribological contacts is well-established in the literature on fretting contacts, mostly in Hertzian type contacts, or in complete contacts that have some type of geometrical discontinuity at the contact edge. The three degradation layers in fretting may be identified as follows; a general deformation layer (GDL), a third body layer (TBL) and TTS [14]. It is assumed that the material in a TTS has undergone plastic deformation that has given rise to a nanocrystalline structure [15] and very high hardness. In fact, the hardness of a TTS is relatively constant regardless of the material used or its initial hardness [16]. Cracks may readily form in a TTS since it is in a totally strain-hardened phase. The elastic modulus remains about the same as that of the bulk material. TTS has been reported to occur in many materials, such as titanium, steels, alloys and coatings [16-19]. It has been reported that slip is needed for TTS to form [20] and that TTS appears after a certain accumulated energy threshold has been exceeded [15]. Once TTS has formed, further energy accumulation contributes to thickening of TTS and generation of wear particles from the TTS layer [15].

The TBL consists of oxidized debris particles. Plastic deformation is expected to occur before the fretting debris is formed. Thus, wear can only be fully understood if one is familiar with the formation of plastic deformation. A TTS has the same basic chemical composition as the bulk material, whereas in the TBL, oxidization has taken place. A TBL may further fragment into smaller particles and the highly oxidized, hard debris acts as a powerful abrasive [21], so this may change the major wear mechanism from adhesive to abrasive.

Millimetre-sized areas of severe fretting damage, 'adhesion spots', have been observed in two fretting test devices with nominally flat-on-flat contacts between self-mated quenched and tempered steel specimens and with only moderate nominal normal pressure [2,22]. These areas under high local

stress have been associated with non-Coulomb friction [2]. Cross-sections made from these locations revealed severe plastic deformation, TTS, TBL and cracking [19]. Even though high-strength quenched and tempered steels are used substantially in highly loaded machine parts, structural steels and cast irons are also widely used materials in assemblies in mechanical engineering. In spheroidal cast irons, graphite is randomly distributed in spheroidal form to preserve beneficial mechanical properties. Structural steels have good strength, stiffness and ductility. Typically, higher strength materials are more susceptible to fretting fatigue than lower strength materials [23].

In this study, frictional behaviour and fretting-induced degradation were experimentally studied using a spheroidal cast iron and a structural steel. The results were compared to previously made quenched and tempered steel tests. The results of the quenched and tempered steel tests have been published earlier [19,24]. A fretting test device having large nominally flat-on-flat contact without discontinuities in sliding direction was used in the experiments. This study will contribute to increased understanding of fretting phenomena in materials commonly used in mechanical engineering. The results could also assist in micromechanical modelling of fretting contact damage.

2. THE EXPERIMENTS

2.1 Materials and test specimen

Spheroidal cast iron EN-GJS-500-7U (hereafter ‘GJS’), structural steel S355 (‘S355’) and quenched and tempered 34CrNiMo6+QT steel (‘QT’) were used in this study. The microstructures of the materials are shown in Figure 1. The measured base material hardness values are as follows: 224HV (GJS), 172HV (S355) and 359HV (QT).

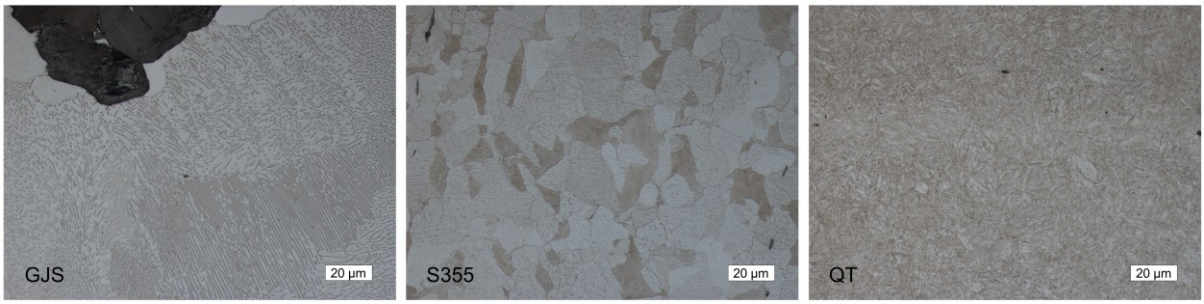

Figure 1. Microstructures of the materials captured with optical microscope, from the left: GJS, S355 and QT.

The inner and outer radiuses of the tubular part of the specimen (Figure 2) are 7.5 and 12.5 mm, respectively, giving an apparent contact area of about 314 mm^2. The contact surfaces of the fretting specimens were ground to surface roughnesses (*Sa*), measured with Wyko NT1100 profilometer, as follows: GJS between 0.1 and 0.18, S355 between 0.16 and 0.18 and QT between 0.2 and 0.32. Circular grinding was applied, producing grinding marks in parallel to the sliding direction.

2.2 Experimental

The three materials were used in three different contact pair combinations using the same test rig and similar nominal operating parameters. GJS-GJS (self-mated) and GJS-S355 tests were carried out and compared to the QT-QT tests. An annular type of flat-on-flat fretting test device previously developed

was used [2] in the experiments. In the device, two axisymmetric specimens are clamped together by normal load, and one specimen is fixed while the second is alternately rotated around the specimen's central axis (Figure 2). Thus, alternating slipping (fretting) is created in the contact.

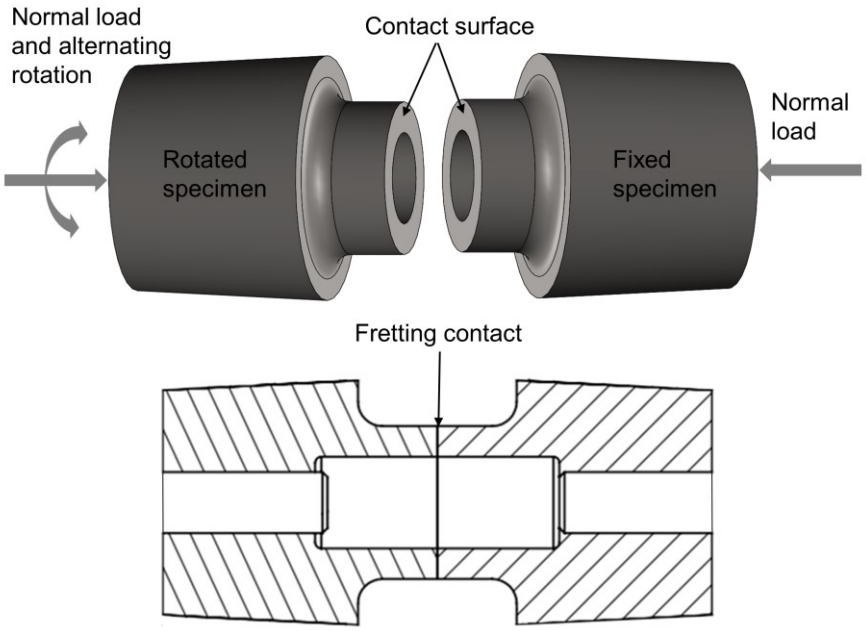

Figure 2. Two annular fretting specimens individually and cross-section of specimens clamped together.

The frictional torque, rotation and normal pressure are measured using a sampling frequency of 5000 Hz. From these measurements, slip in the contact and *COF* in gross sliding can be evaluated. In addition, the sliding regime can be indicated by the 'fretting loops', i.e., the plot of frictional torque against rotation, which is recorded throughout the tests. The *COF* can be determined in two ways [2]. COF_{max} is determined in gross sliding from the maximum frictional torque during a loading cycle and the normal pressure distribution, thus representing the maximum coefficient of friction, whereas COF_{mean} is the average *COF* and is calculated from the frictional energy dissipation, represented by the area inside the fretting loop, and the rotation amplitude. The difference between COF_{max} and COF_{mean} represents the level of non-Coulombness, since the higher is the 'hook' in the fretting loop around the reversing point in non-Coulomb friction conditions, the greater is the difference between these two *COF*s. Hintikka et al. [2] found that it is better to use two *COF*s to capture frictional behaviour comprehensively. Rotation in the test device is measured at some distance from the contact, but elastic deformations are removed to determine the actual slip between the specimens at the contact interface. The sliding amplitude reported here is determined using the mean radius (10 mm). Because of the annular geometry, the sliding amplitude decreases towards the inner radius and increases towards the outer radius from the mean radius. The normal pressure has a rather linear distribution, being highest at the inner annulus and having a maximum range of deviation of about ±18% from the nominal value. This was determined numerically in [25].

In all the experimental tests reported here, the test scheme was similar for all the material and contact pairs. Two types of test were made: gross sliding tests and tests below fully developed friction, i.e., so called *TR* tests [25]. The nominal normal pressure in all tests was 30 MPa. The gross sliding tests had a sliding amplitude of 35 μm. In *TR* tests, only a portion of friction is used to determine the

threshold for unstable frictional behaviour [25]. These tests result in limited fretting damage and typically average sliding amplitudes in the range of only a few micrometers. *TR* refers to traction ratio and it is analogous to normalized tangential force, i.e. the tangential force divided by the normal load in linear sliding. *TR* corresponds to COF_{max} in gross sliding conditions. A fuller description of the *TR* test scheme is given in [25]. The analysed tests, including the number of tests, are presented in Table 1.

Table 1. Analysed tests.

Gross sliding tests

Material pair	Loading cycles [-]	Normal pressure [MPa]	Sliding amplitude [μm]	Number of tests [-]
GJS-GJS	3×10^6	30	35	3
GJS-S355	3×10^6	30	35	2
QT-QT	3×10^6	30	35	2

TR tests

Material pair	Loading cycles [-]	Normal pressure [MPa]	*TRM* [-]	Number of tests [-]
GJS-GJS	3×10^6	30	0.44-1.01	6
GJS-S355	3×10^6	30	0.49-0.95	4
QT-QT	3×10^6	30	0.28-0.94	6

The fretting loading frequency was 40 Hz. In previously performed QT-QT experiments, the rotation amplitude was increased from zero to the desired value during 400 loading cycles. Therefore, the same length startup phase was used with the GJS-GJS and GJS-S355 tests. There were a total of three million loading cycles. The tests were carried out in dry contact conditions, and before testing the specimens were cleaned in an ultrasonic bath, first with acetone and then with ethanol. Contact alignment was confirmed by adjusting uniform normal pressure distribution using Fujifilm pressure-sensitive film before each test. The tests were carried out in normal laboratory conditions.

2.3 Characterization methods

The cross-sections enable the assessment of the fretting-induced damage, i.e., the degradation layers and cracking below the contact surface. Cross-sections were taken at locations that were suspected of being the remnants of ‘adhesion spots’ [2,19] or at locations that displayed a high level of surface degradation under visual inspections based on surface optical microscopy, Figure 3. The focus was on the centre annulus of the contact.

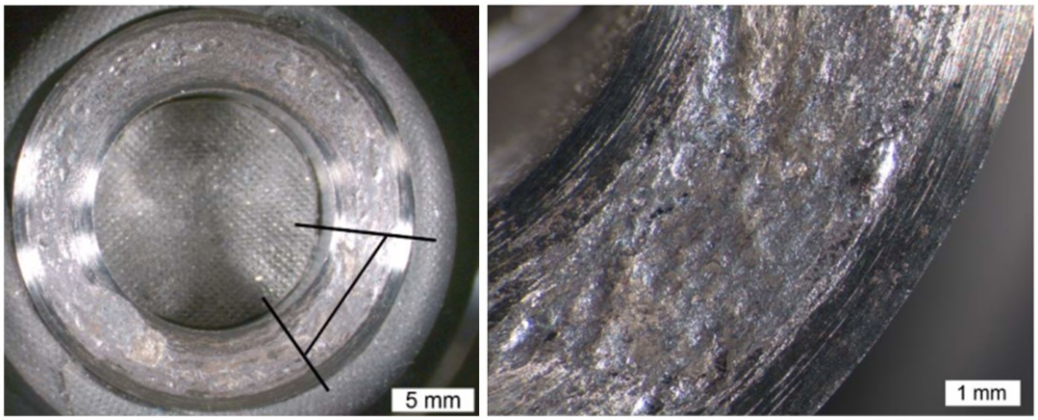

Figure 3. Example of a cross section location on the fretted contact surface.

After the fretting experiments, the samples were then washed with mild acid detergent to remove fretting debris from the surface. After contact surface documentation with an optical stereo microscope, the cut samples were mounted on a thermoset with carbon additive. The cross sections were ground and polished. Etching was made in 4% Nital (nitrid acid HNO_3 solved in ethanol). The cross-sections were studied using an optical microscope (Leica DM 2500M) and a field emission scanning electron microscope (FESEM, Zeiss ULTRAplus) equipped with an energy dispersive spectrometer (EDS, Oxford Instruments XMaxN) and with an electron backscatter diffraction (EBSD, Oxford Instruments Symmetry) system. For EBSD measurements, the cross-sectional samples were prepared by molding the cut sample into epoxy and then by grinding and polishing. After polishing, the samples were removed from the epoxy molding.

3. RESULTS

Inspection of the contact surfaces after testing revealed the presence of fretting damage regardless of the material used in the contact pair. As expected, the most severe fretting scars were observed in the gross sliding tests, Figure 4. Essentially, in the gross sliding tests the entire nominal contact area lay under fretting scar, whereas in the *TR* tests only a limited amount of fretting damage was observed and significantly large areas remained undamaged. This was evidenced by the fact that manufacturing marks were still evident (the scars are shown below in Figure 13 and Figure 14).

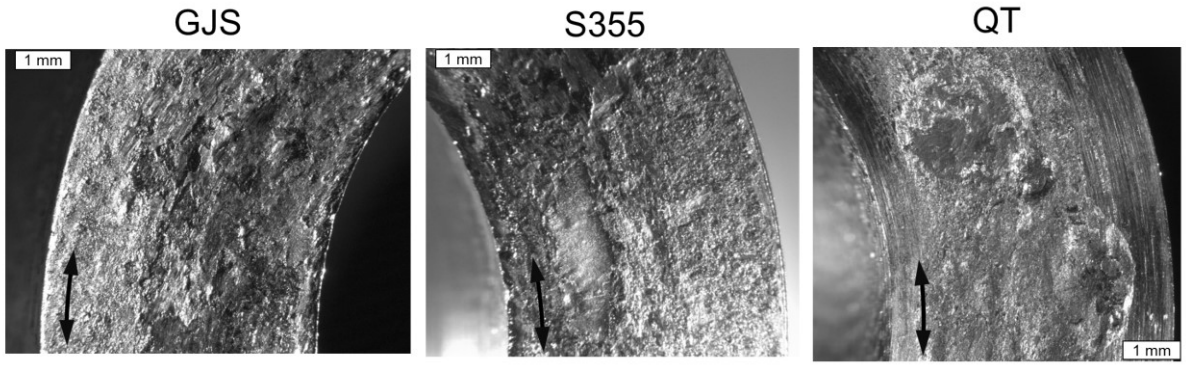

Figure 4. Images of contact surfaces taken with a stereomicroscope after gross sliding tests. The arrows show sliding direction.

3.1 Frictional behaviour

The evolution of COF_{max} and COF_{mean} for the GJS-GJS, GJS-S355 and QT-QT contacts during the three million loading cycles are shown in Figure 5. The start-up phase (the first 400 loading cycles), during which slip is still increasing, is marked in the graphs.

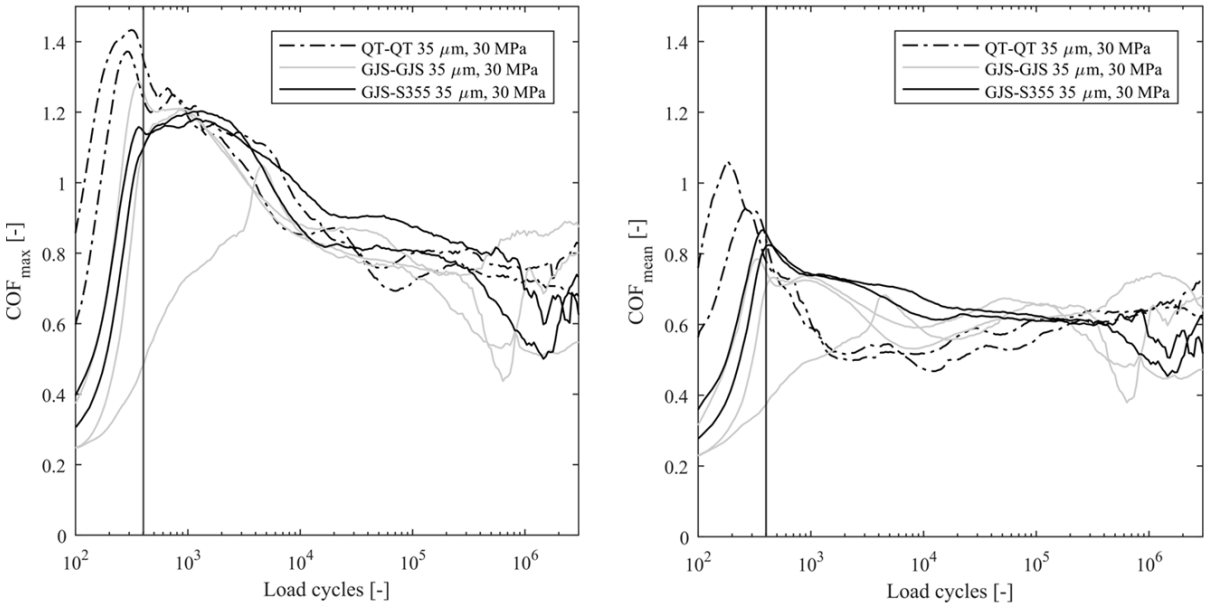

Figure 5. COF_{max} and COF_{mean} in gross sliding tests.

Regardless of the contact material pair, the *COFs* peak at the beginning of the tests and then stabilizes after some tens of thousands of loading cycles. The maximum value for COF_{max} occurs with QT-QT, and is 1.43. The corresponding values for GJS-GJS and GJS-S355 are 1.29 and 1.20, respectively. The average value of stabilized COF_{max} is about 0.7. The friction peak occurs somewhat earlier in QT than in GJS and S355. According to the difference between COF_{max} and COF_{mean}, the highest level of non-Coulombness is observed with the QT-QT pair while the non-Coulombness is somewhat lower with GJS-GJS and GJS-S355, both of which have rather similar levels. Overall, frictional behaviour is fairly similar among the different material pairs in gross sliding conditions. Fretting loops around the locations of friction peak (A) and stabilised friction (B) for all the material pairs are shown in Figure 6.

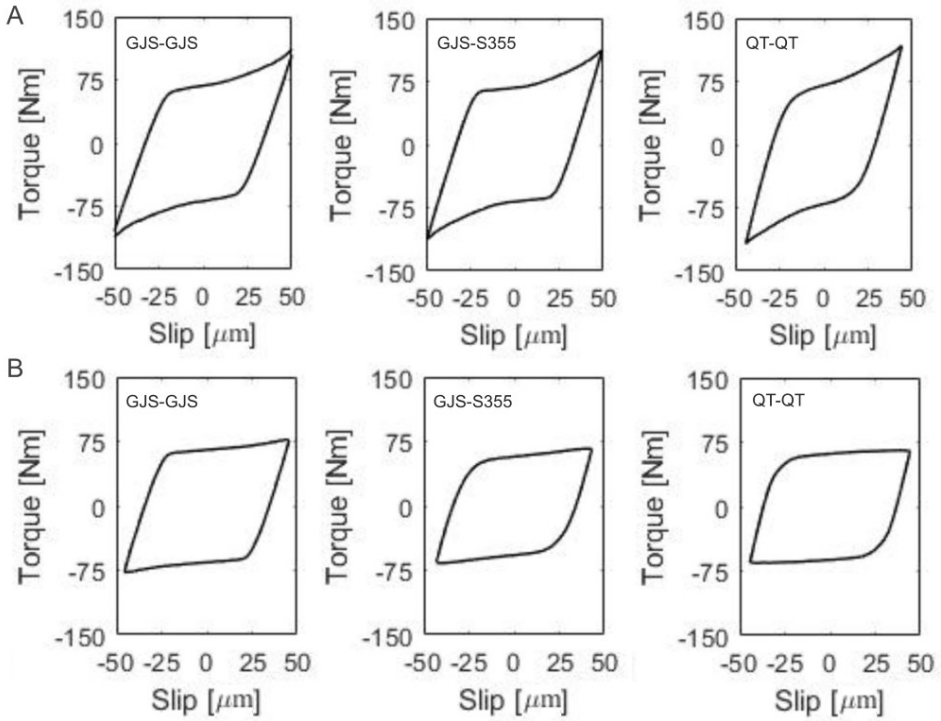

Figure 6. Measured fretting loops of gross sliding tests, around friction peak (A) and stabilized friction (B).

Overall, similar behaviour can be observed in the fretting loops in gross sliding conditions between the material pairs. In all the pairs, a "hook-shaped" fretting loop around the friction peak (A) reveals non-Coulomb frictional behaviour, where torque increases when the turning point is approached. At stabilized *COF* phase (B), this shape of the loops is revealed as being somewhat rectangular and the torque is notably more constant during the gross sliding phase.

Figure 7 shows the frictional behaviour of the *TR* tests, i.e., tests with limited utilization of friction. The maximum value of the traction ratio (*TR*) during testing is referred to as *TRM*. *TRM* values were between 0.28-0.94 (QT-QT), 0.44-1.01 (GJS-GJS) and 0.49-0.95 (GJS-S355) in the tests.

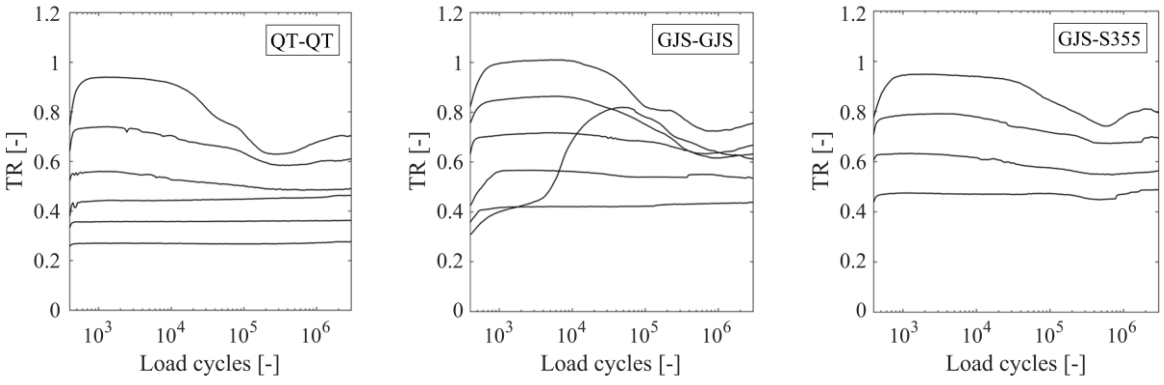

Figure 7. Traction ratio (TR) curves of QT-QT [25]*, GJS-GJS and GJS-S355 contact pairs.*

Overall, the behaviour between the contact pairs is similar. In QT-QT, the threshold for stable friction was found to be about 0.5 [25]. This means that when *TR* is higher, friction starts to peak at the beginning, and this leads to unstable frictional behaviour. In all the tests with *TR* levels lower than about 0.5, friction is basically stable (constant) throughout the test. As *TR* increases, friction starts to

peak initially, leading to unstable frictional behaviour. This threshold seems to be at similar levels in all the material pairs. In addition, the stabilized *TR* values show similar behaviour and values between the material pairs. However, further tests are needed to determine the threshold more reliably and precisely. In the GJS-GJS pair there is an interesting curve (*TRM*=0.82) displaying low friction during the first few thousands of loading cycles, which then increases and stabilizes to a value similar to the other curves. Indeed, a similar kind of behaviour was observed in one gross sliding test. This may be related to the graphite-induced tribological properties of cast-iron, which may cause a decrease in friction due to improved lubrication [26]. Figure 8 shows examples of fretting loops of *TR* tests at the end of the tests with low (A) and big (B) *TR* values.

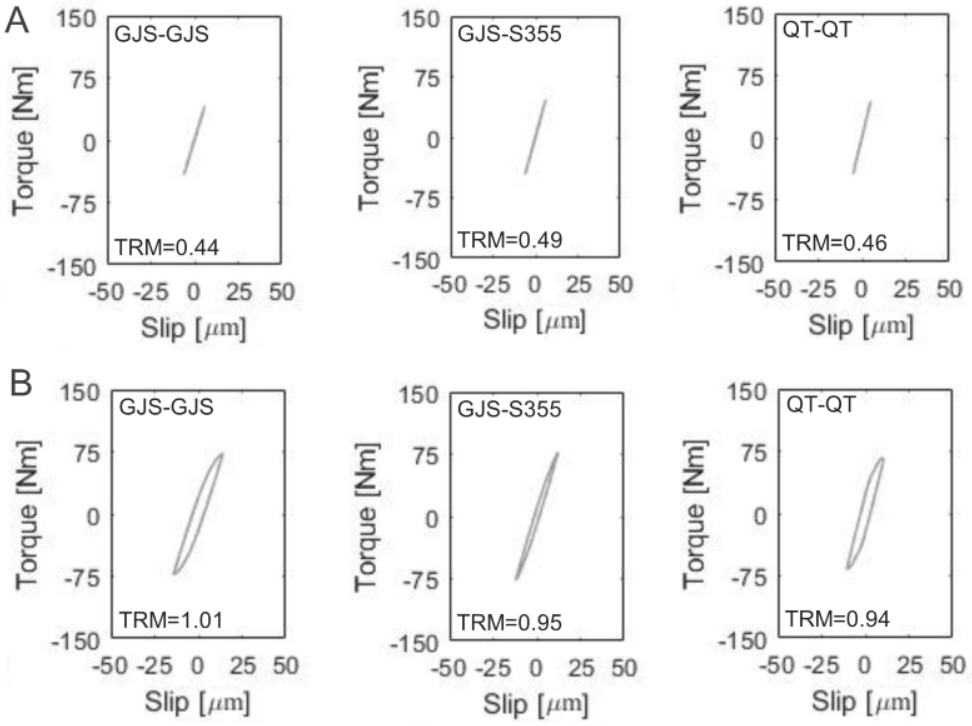

Figure 8. Measured fretting loops of TR tests, low (A) and high (B) TR-level.

The loops at the lowest *TR* levels (*TRM* 0.44–0.49, A) of all materials are narrow, indicating stick or a minimal partial slip running condition. At higher *TR* levels (*TRM* 0.94–1.01, B), the frictional energy is dissipated and the contact is in partial/gross sliding condition, with a sliding amplitude of around a few micrometres. Similar frictional behaviour is observed from the fretting loops between the material pairs.

3.2 Degradation layers

3.2.1 Gross sliding tests

FESEM-images from the cross-section of a GJS-GJS gross sliding sample are shown in Figure 9.

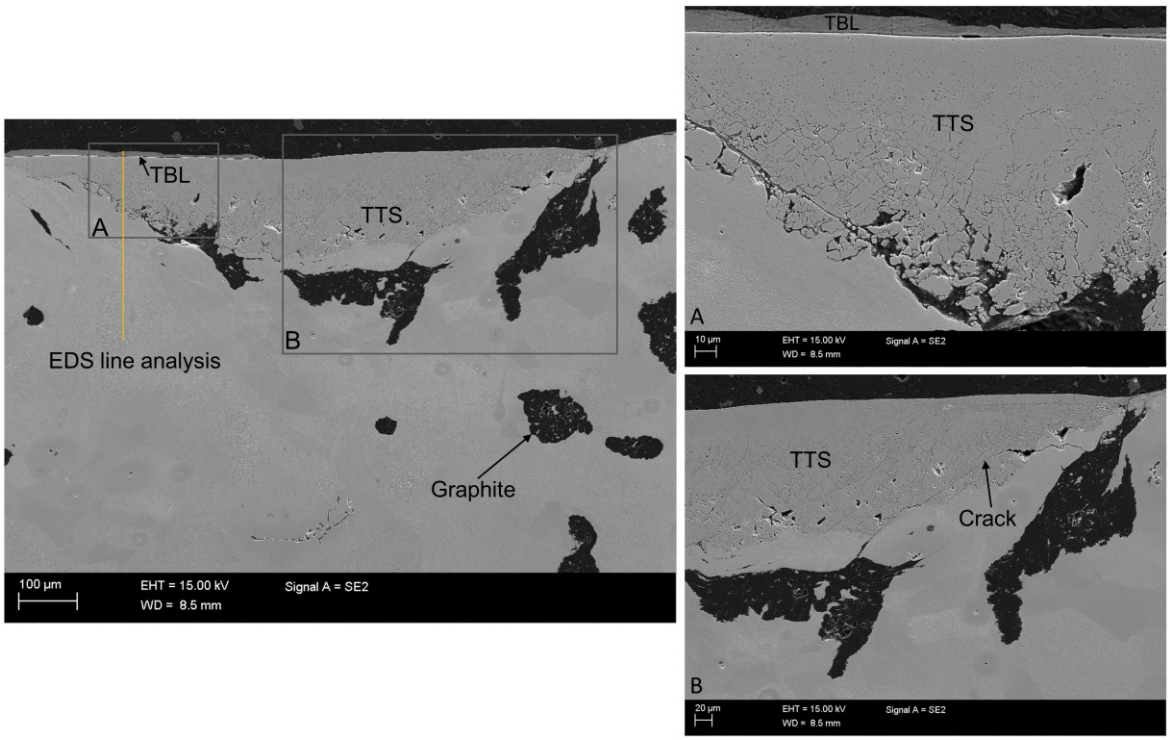

Figure 9. FESEM images showing fretting-induced damage in GJS (GJS-GJS contact).

Degradation layers can be observed, together with crack, at both edges of the degraded region. The TBL layer can be identified by the high amount of oxygen; the EDS results are shown later on in Figure 12. The TBL layer in this figure is a rather thin layer over the TTS. The TTS layer is about 170 µm thick and it seems to be bounded by graphite.

Although the TBL and the TTS are both porous, their appearance is different, as the TTS layer has a highly cracked structure (Figure 9). In QT, the cracks in TTS run at a remarkably constant angle of 45° [19], whereas in GJS there is virtually no discernible pattern to the structure, i.e. the cracks have random paths (Figure 9). The hardness of the TTS layer in QT was measured as being very high, over 1000 HV, and since the hardness is higher than for a totally work-hardened material, it may easily crack. Hardness measurements were taken from two samples of both GJS and S355 (six locations in total). Figure 9A shows how the TTS layer nearer the surface (up to about 50 µm) has a denser structure than in the lower region, which is more heavily cracked. This is clearly reflected in the measured hardness values. The average hardness of the TTS closer to the surface is 758HV0.05, while in the lower region it is 483HV0.05. The average hardness of TTS in S355 is 578HV0.05 and 521HV0.025. The results show that the hardness values are much higher in the degraded region, though they are lower than for QT. The change from TTS to TBL (Figure 9A) is clearly delineated. Similar behaviour was observed with S355 and also with QT. The hardness of TBL in QT was about 700 HV, which is a typical value for porous oxide layer. TBL is most likely formed by sintering, where micrometer sized particles adhere together to produce a porous structure. The TBL layers of GJS and S355 were too thin to be measured.

The deformation of material was examined using EBSD measurements. Figure 10 shows images collected by a forward scattered electron detector (FSD) on the EBSD detector and normal direction inverse pole figure (IPF) orientation maps superimposed on band contrast (BC) maps.

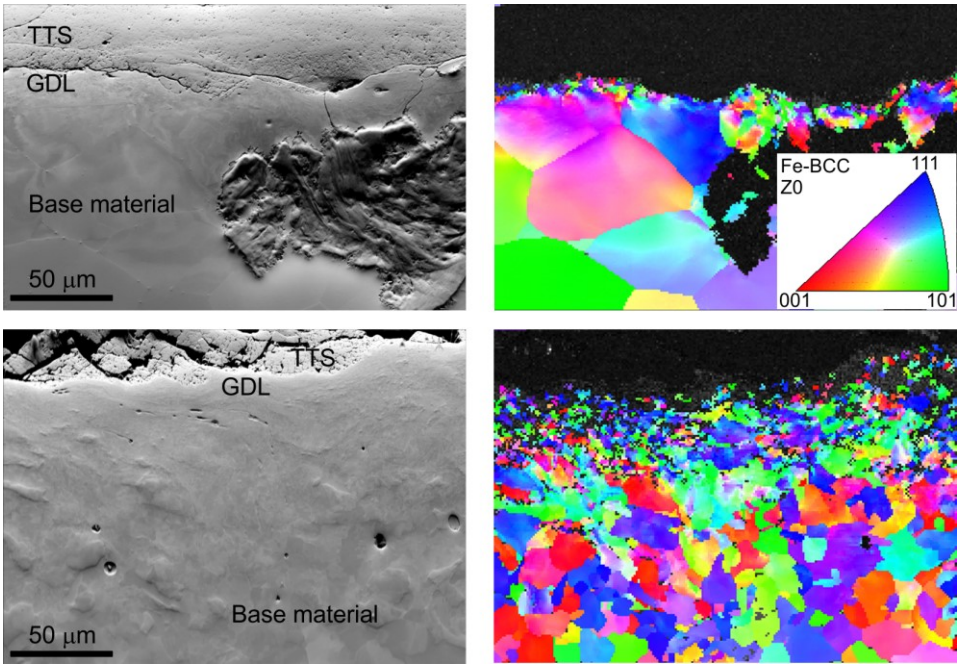

Figure 10. FSD images and normal direction IPF maps superimposed on a BC map, GJS (upper) and S355 (lower). (For interpretation of the references to color in this figure legend, the reader is referred to the Web version of this article.)

As Figure 10 shows, neither the TTS nor the TBL layers can be indexed as Fe-BCC, either because of the high degree of plastic deformation, the excessively refined microstructure or phase transformation. However, indexing is possible at the GDL. Both materials at the GDL have smaller grains than the base material. This was also the case in QT. Indexing improves as one moves towards the base material, indicating that the level of plastic deformation also decreases. In this case, the depth of material degradation is quite similar for both the GJS and S355.

The fretting-induced damage in GJS for both the GJS-GJS and GJS-S355 tests was fairly similar, as were the appearance and size of the degradation layers, and the cracking. In this case, therefore, the different contact pairs do not seem to have had much effect, even though greater damage might have been expected due to the increased adhesion when similar materials are in contact. Figure 11 shows the degradation in S355 and GJS. In general, the depth of the degradation layers and the cracks in S355 are smaller than in GJS and QT. The microstructure is highly distorted close to the contact interface. Evidence of plastic deformation can be seen from the orientation of the microstructure.

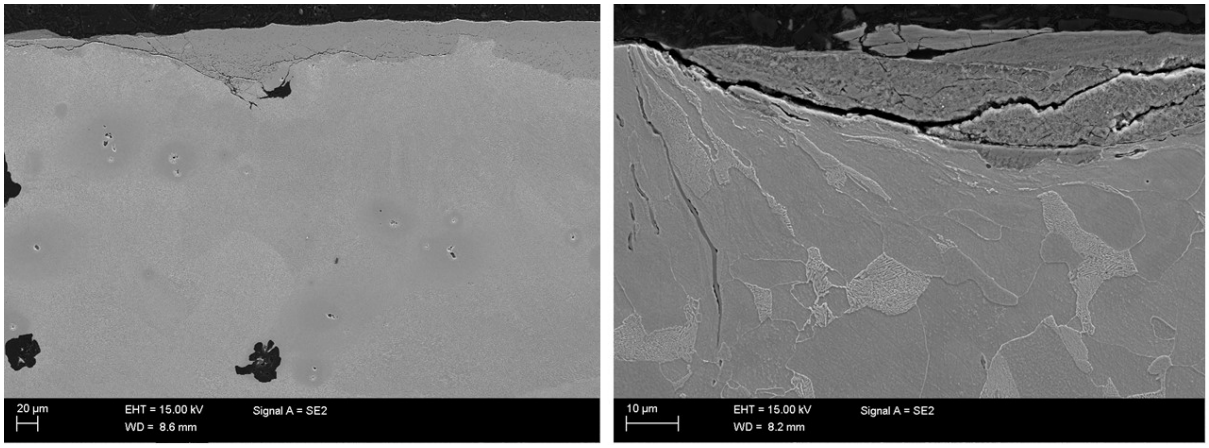

Figure 11. Degradation and cracking in GJS (on the left) and S355 (on the right) in GJS-S355 gross sliding test.

TBL can be indicated by the oxygen content [27]. Figure 12 shows the EDS line analysis results for GJS (Figure 12A) and S355 (Figure 12B). The location of the EDS line in Figure 12A is also shown in Figure 9.

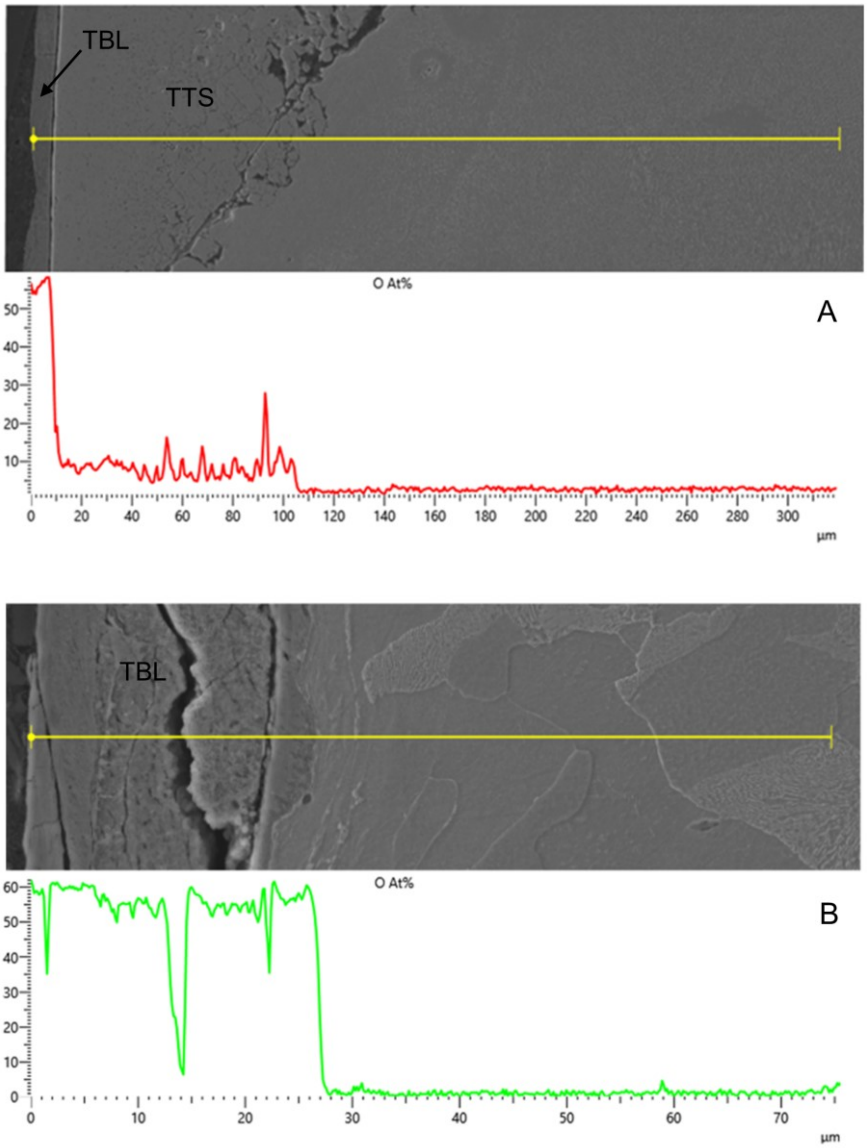

Figure 12. FESEM image and EDS line analysis of oxygen for GJS (A) and S355 (B).

The thin TBL layer (about 10 µm) on the TTS in Figure 12A has a high oxygen content.. In Figure 12B, the TBL layer having an oxygen content at a similar level exists on the deformed microstructure, without the TTS layer. In this case, the TBL layer is thicker in Figure 12B than in Figure 12A. The oxygen content in these samples is greater than that measured with QT. Since the TTS contains non-oxidized steel, the formation of oxides cannot explain the increased hardness in TTS.

3.2.2 Tests below fully developed friction

Fretting-induced damage in *TR* tests is presented in Figure 13 (GJS-GJS) and Figure 14 (GJS-S355).

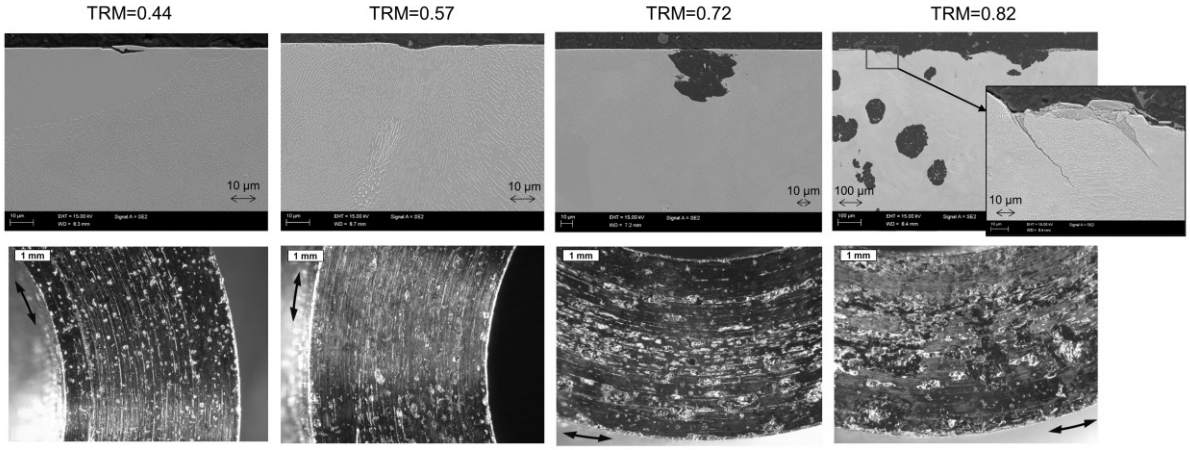

Figure 13. Fretting-induced damage in the tests below fully developed friction, GJS-GJS contact. TR and slip increases from left to right. Corresponding fretting scars are shown below the cross-sections. Arrows indicate the sliding direction.

The optical microscope images of the fretting surfaces reveal that only a limited amount of fretting wear and damage has occurred (bottom row in Figure 13). The contact surfaces with low *TR* ratios still have manufacturing (grinding) marks clearly visible and the fretting scar covers only a minor portion of the surface. The higher the *TR*, the larger is the coverage of the fretting scar. With the highest *TR* level (0.82), much more severe fretting damage can be observed on the surface, resembling the surface damage observed in gross sliding tests. This is also reflected in the sub-surface damage, as shown in the upper row of Figure 13. Clearly-formed degradation layers and cracking are observed only with the highest *TR* level. Indeed, with the same *TR* level, the crack length is comparable to crack lengths of QT [24]. Only small cracks, some micrometers in length are observed with *TR* values of 0.57 and 0.72. With lower *TR* values, clear orientation of perlite can be seen very close to the contact surface, which is evidence of plastic deformation. This may have been caused by fretting loading, but could possibly have already occurred during the manufacture of the specimen. With the lowest *TR* level, a “chip” was found on the surface, which may be attributable to fretting-induced shear loading. The corresponding *TR* test results for the GJS-S355 pair are shown in Figure 14.

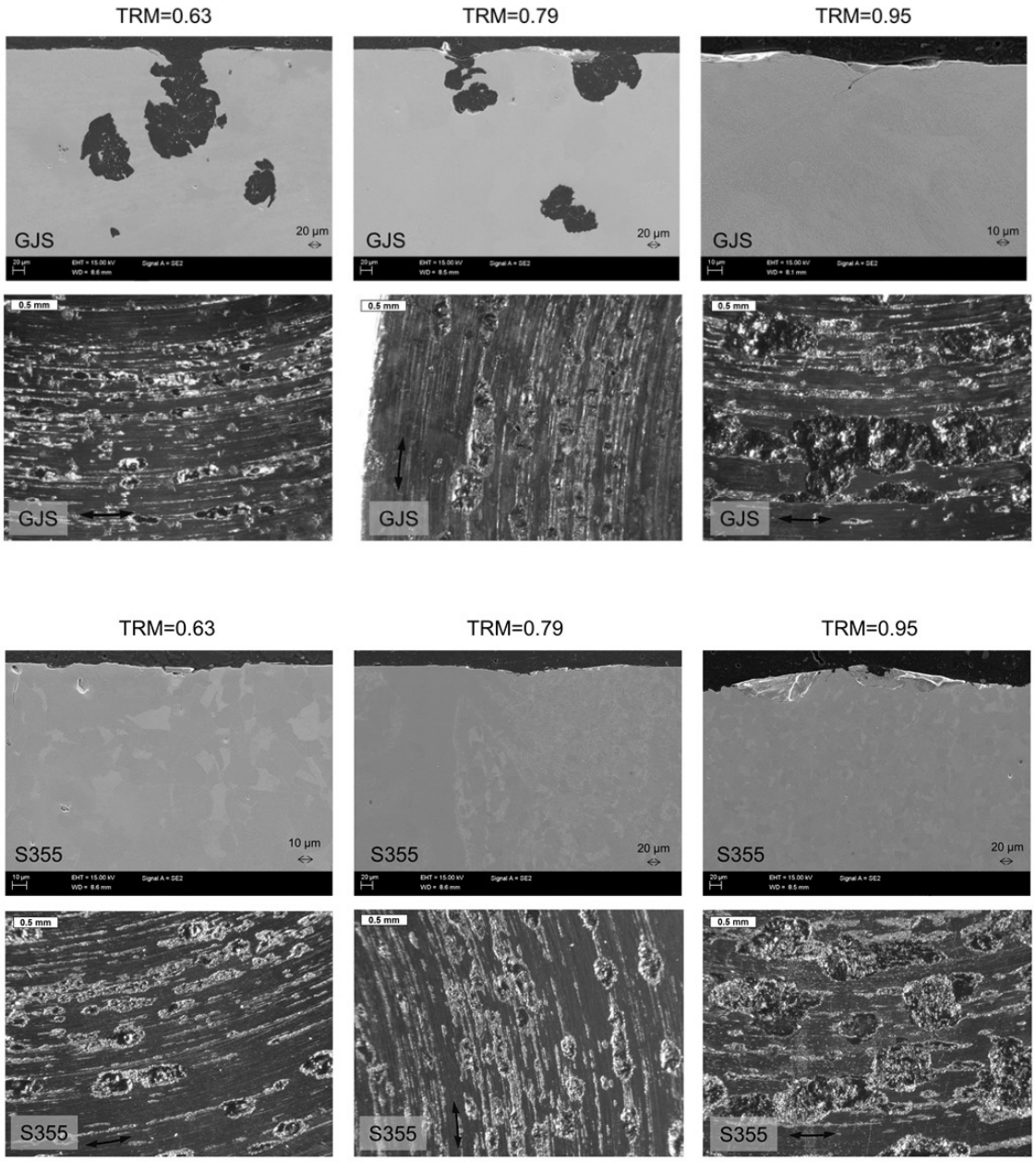

Figure 14. Fretting damage in the tests below fully developed friction, GJS-S355 contact. Above GJS and below S355. TR and slip increases from left to right. Sliding directions are marked by arrows.

A similar pattern of behaviour is observed here. The contact surface damage increases as *TR* is increased and the most severe damage is observed with the highest value of *TR*M, being 0.95 in this case. Within this value, cracking can clearly be seen, although they are only a few tens of micrometers long. Smaller cracking and a thin degradation layer can already be observed with the lowest value of *TR* (0.63). Nevertheless, a *TR* level of 0.95 seems to be needed to form clear degradation layers. In addition, in the *TR* tests the degradation layers occur only over a narrow width, whereas in the gross sliding tests a larger proportion of the cross-section is covered. The *TR* value of 0.95 corresponds to the maximum average sliding amplitude of about 2.3 µm during the test. Within the test contact, partial slip with low sliding amplitudes can occur in such a way that the inner annulus gets stuck and the outer annulus is sliding. However, this kind of behaviour was not observed in any of the GJS, S355 or QT specimens.

3.3 Cracking

As shown previously, fretting-induced cracking was observed in the cross sections. Clearly bigger cracks exist in the gross sliding samples than in the *TR* tests. Dominant cracks could be observed at the edges of the most degraded region, but there were also smaller cracks. In GJS, at some points the cracks followed the distribution of graphite, meaning that graphite can affect the crack propagation path. Figure 15 shows typical damage in GJS and S355, representing quite comprehensive damage observed throughout the contact. Overall, in S355, rather than having locations with a relatively long crack pair, shorter and shallower crack 'chips' exist, as seen in Figure 15. These could become detached as wear particles.

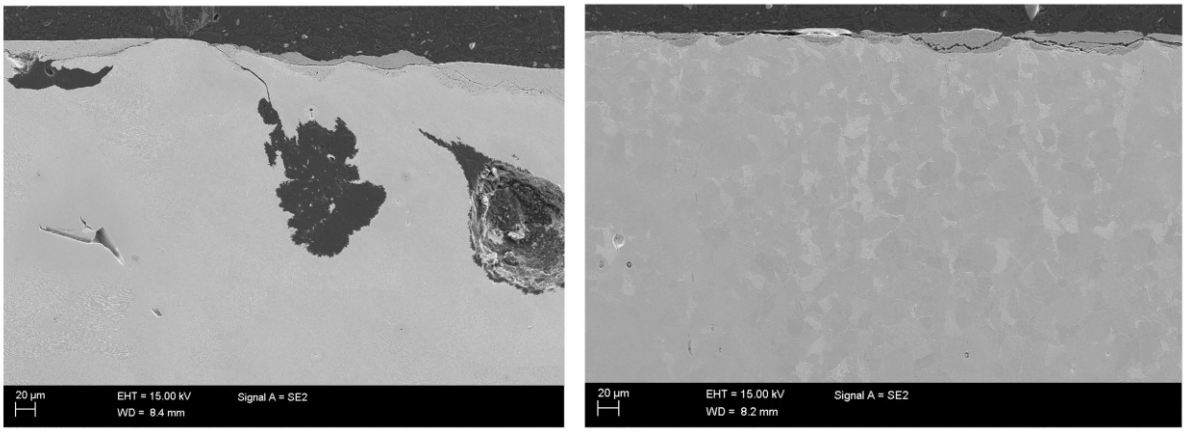

Figure 15. FESEM images showing typical damage in GJS and S355.

Cracks occurred at the sides of the degraded region in all the materials. The maximum measured lengths of cracks in GJS and S355 were about 230 µm and 100 µm, respectively. Crack lengths and depths of about 980 µm and 470 µm were measured for QT with the same sliding amplitude and normal pressure [24], so it is clear the dimensions of the cracks observed within GJS and S355 were much smaller than for QT. The average angle of a crack to the contact surface is 26.9° in GJS. This angle corresponds to the angle measured for QT, when all tests in different operating conditions were considered [24]. With QT, this angle was quite independent of the operating conditions. In S355, the corresponding angle was lower. However, it was observed in QT that the angle is often shallower close to the contact, the angle being increased further away. As the crack lengths were considerably shorter in S355, the measured smaller angle seems to be within some agreement with QT at the same crack lengths.

4. DISCUSSION

Severe fretting-induced damage in terms of plastic deformation, TTS and TBL layers and also cracking were observed in all three different material contact pairs studied here. The various contact pairs were tested in the same fretting device and within the same nominal operating parameters. The cross-sections were made at the fretting scar, usually at the radius in the middle of the contact. The debris ejection rate from the contact may be assumed to increase closer to the inner and outer edges, and presumably debris will persist longer nearer the centre. The most extensive damage and cracking was observed in the cross-sections from the QT-QT pair. With QT-QT, the area of severe plastic deformation was the largest and the crack length the longest. The maximum thickness of the TTS

layer was measured in GJS, but the thickness was comparable with QT. S355 had the lowest measured thickness, and also the smallest number of visible cracks. Change in grain orientation to the sliding direction was observed even in the *TR* tests with limited fretting loading. The material directly below the TBL/TTS layer was characterized by finer microstructure in all materials.

Dominant cracks were observed at the edges of the damaged regions, though cracks were also observed elsewhere. Surface-oriented 'chipping' was evident with S355 instead of long cracks propagating inside the material, which was observed with GJS and especially with QT, characterized by 'crack pairs'. The size of plastic deformation and crack dimensions may indicate that fretting-induced contact stresses have a deeper impact in QT compared to GJS and S355. In contrast, ferrite as the tougher phase may display fewer changes under plastic deformation than martensite. Nevertheless, the growth of cracks is restricted to within the region of contact induced loading, as the nominal torque due to the rotation is not in itself high enough to prolong crack growth [24]. Though graphite is distributed throughout the GJS, in many places it occurs in the crack propagation path and close to the regions of damage. This suggests that graphite may have an effect on damage formation in GJS.

The concept of stable and unstable friction was developed by Hintikka et al. [25]. Using a QT-QT contact pair, the authors showed that visual surface damage was limited below the determined threshold [25] and this also applied to the sub-surface damage [24]. Comparable results that support their findings were observed in the present study using GJS and S355. The results for all materials showed that when friction behaviour was unstable, i.e., a peak at the beginning of testing, this also led to the formation of degradation layers and cracking. The amount of damage in terms of fretting scar increased as the *TR* increased and it was most clearly visible in gross sliding conditions. The measured fretting loops were very narrow at low *TR* levels, but at higher levels the loops clearly displayed increased frictional energy dissipation. As all the material pairs also displayed an initial friction peak and stabilization to a lower value in gross sliding conditions, the different contact material pair does not seem to have any major effect on frictional behaviour.

With QT, millimetre-sized cracks had already formed early in the loading history when the coefficient of friction was high. Higher levels of initial friction may be related to more extensive damage. The highest initial *COF* was measured for QT-QT, and the maximum value of *COF* was lower in both the GJS-GJS and GJS-S355 contacts than in QT-QT. This may indicate that adhesion is lower, which may be one reason that less damage was observed in GJS and S355, at least in terms of the extent of the plastic deformation and cracking. The friction peak in fretting is related to adhesive friction. With QT, short duration tests were done that show evidence of adhesion. In tribological terms, as the GJS-S355 pairs had different materials in contact, they may have the lowest level of adhesion in sliding and therefore, probably, the lowest initial friction peak. The presence of graphite on the contact surface may act as a solid lubricant and therefore decrease friction. The friction peak occurs slightly earlier in QT than in GJS and S355. This may be related to the quicker dispersal of the oxide surface layers, which leads to a more rapid increase in adhesion. With regard to the gross sliding tests presented in Figure 5, the highest cumulative frictional energy dissipation measured during the tests

was for the QT-QT pair, being about 10% higher than in the GJS-GJS pair, which in turn has an almost 10% higher value than the GJS-S355 contact pair. This at least partly correlates with surface damage but, of course, the value relates to the entire contact and does not reflect local behaviour.

With the contact surfaces in Figure 4, more clearly discernible “adhesion spots” are created in the QT-QT contact, i.e., clear points of severe localized damage. In GJS-GJS and GJS-S355, by contrast, somewhat more even wear is observed, as the entire nominal contact area is covered by the fretting scar. However, since contact surfaces were inspected after three million of cycles, the remnants of adhesion spots created at the start of testing could have been worn away. In QT, however, such spots could have been more easily visible due to less wear. One explanation for this different behaviour may relate to the real area of contact. As the surfaces are brought into contact, some tips of surface roughness contact, and then deform plastically as the load is increased. As more and more asperities deform in this way, the real area of contact increases along with an increase in load. Regarding the strength and hardness values of the materials, the real area of contact is possibly greater in GJS and S355. In QT, the loading could be concentrated more locally. In addition, on the basis of the two cross section samples that were imaged thoroughly with SEM, the TBL layer in S355 extended almost across the entire contact surface. This can act as a protective layer against fretting damage, which may partly account for the decreased level of damage.

In general terms, the use of materials having higher strength allows the design of lighter structures. However, in this study the quenched and tempered steel pair had the longest cracks. The tensile strengths of the GJS and S355 used are at a similar level though the yield strength is somewhat higher for the S355. However, QT has much higher strength values. As a result, the adhesive junctions may break more easily in GJS and S355 than in QT, whether due to monotonic or fatigue loading. This may restrict crack growth in GJS and S355 compared to QT.

An annular type of flat-on-flat fretting test device was used having a large nominal contact area, and which emulates the actual contacts in machine components. The local millimeter-sized spots underline the importance of large-scale laboratory contact since such behaviour may not be observed when using smaller laboratory test geometries. However, such non-idealities may also be encountered in practical contacts. Important further action is to study the actual local conditions in terms of stresses and strains.

5. CONCLUSIONS

This study focused on fretting-induced material degradation at adhesion spots, and frictional behaviour. A comparison was made between cast iron, structural steel and quenched and tempered steel under similar testing conditions. A fretting test device having a large flat-on-flat contact was used in the experiments with only a moderate nominal normal pressure and different sliding conditions.

All the tested material pairs had severely deformed microstructures with refined and oriented grains. The major changes to the materials occurred at the contact surface or in its close vicinity, and decreased the nearer one gets towards the base material. The deformed microstructure extended

deepest in the case of quenched and tempered steel, being some hundreds of micrometers. Tribologically transformed structures (TTS) that were about three times as hard as the base material and a third body layer with oxidation levels of about 60% were observed in all the materials. Cast iron and quenched and tempered steel had thicker TTS layers than the structural steel, with values typically ranging from a few dozen micrometers up to a couple of hundred micrometres. In the tests below fully developed friction (i.e., *TR* tests), the TTS was only a few micrometers thick. Cracks developed mainly in gross sliding conditions, but also in the *TR* tests, though the dimensions of the cracks in the *TR* tests were considerably smaller than the cracks occurring in gross sliding conditions. The longest cracks were seen with quenched and tempered steel, and some of these were well over a millimetre in length. The frictional behaviour of all the material pairs was characterized by a peak in the coefficient of friction during the initial loading cycles in gross sliding conditions. This peak was about 20% higher with quenched and tempered steel than it was with cast iron and structural steel. This peak was followed by stabilization at values around 0.7 in all the materials. The threshold for unstable friction was about 0.5 for all the materials studied.

6. ACKNOWLEDGEMENTS

The authors are grateful for the financial support provided by Business Finland Oy (formerly Tekes) in the form of research projects ISA (Dnro 7204/31/2018), WIMMA Dnro 1566/31/2015 and MaNuMiES (Dnro 3361/31/2015) and Wärtsilä Finland Oy. The FESEM-EDS-EBSD work made use of Tampere Microscopy Center facilities at Tampere University. Enni Luoma and Leevi Kurki carried out the preparation of the test specimens for microscopic characterization.

7. REFERENCES

[1] Hills DA, Nowell D. Mechanics of Fretting Fatigue. Dordrecht: Kluwer Academic Publishers; 1994.

[2] Hintikka J, Lehtovaara A, Mäntylä A. Fretting-induced friction and wear in large flat-on-flat contact with quenched and tempered steel. Tribol Int 2015;92:191–202. https://doi.org/10.1016/j.triboint.2015.06.008.

[3] Leidich E, Maiwald A, Vidner J. A proposal for a fretting wear criterion for coated systems with complete contact based on accumulated friction energy density. Wear 2013;297:903–910. https://doi.org/10.1016/j.wear.2012.11.006.

[4] Pape JA, Neu RW. A comparative study of the fretting fatigue behavior of 4340 steel and PH 13-8 Mo stainless steel. Int J Fatigue 2007;29:2219–2229. https://doi.org/10.1016/j.ijfatigue.2006.12.016.

[5] Hintikka J, Juoksukangas J, Lehtovaara A, Frondelius T, Mäntylä A. Non-idealities in fretting contacts. J Struct Mech 2017;50:171–174. https://doi.org/10.23998/rm.64886.

[6] Niva J. An examination of the propagation of fretting cracks using fracture mechanics. J Struct Mech 2017;50:186–190 (in Finnish). https://doi.org/10.23998/rm.64935.

[7] Mäntylä A, Göös J, Leppänen A, Frondelius T. Large bore engine connecting rod fretting analysis. J Struct Mech 2017;50:239–243. https://doi.org/10.23998/rm.64914.

[8] Conner BP, Hutson AL, Chambon L. Observations of fretting fatigue micro-damage of Ti-6Al-4V. Wear 2003;255:259–268. https://doi.org/10.1016/S0043-1648(03)00152-2.

[9] Wallace JM, Neu RW. Fretting fatigue crack nucleation in Ti-6Al-4V. Fatigue Fract Eng Mater Struct 2003;26:199–214. https://doi.org/10.1046/j.1460-2695.2003.00553.x.

[10] Szolwinski MP, Farris TN. Observation, analysis and prediction of fretting fatigue in 2024-T351 aluminum alloy. Wear 1998;221:24–36. https://doi.org/10.1016/S0043-1648(98)00264-6.

[11] Waterhouse R. Fretting corrosion. Oxford: Pergamon press; 1972.

[12] Fellows LJ, Nowell D, Hills DA. On the initiation of fretting fatigue cracks. Wear 1997;205:120–129.

[13] Pape JA, Neu RW. Subsurface damage development during fretting fatigue of high strength steel. Tribol Int 2007;40:1111–1119. https://doi.org/10.1016/j.triboint.2006.10.009.

[14] Li J, Lu Y, Zhang H, Xin L. Effect of grain size and hardness on fretting wear behavior of Inconel 600 alloys. Tribol Int 2015;81:215–222. 10.1016/j.triboint.2014.08.005.

[15] Fouvry S, Liskiewicz T, Kapsa P, Hannel S, Sauger E. An energy description of wear mechanisms and its applications to oscillating sliding contacts. Wear 2003;255:287–298. 10.1016/S0043-1648(03)00117-0.

[16] Zhou ZR, Sauger E, Liu JJ, Vincent L. Nucleation and early growth of tribologically transformed structure (TTS) induced by fretting. Wear 1997;212:50–58. 10.1016/S0043-1648(97)00141-5.

[17] Peteghem B Van, Fouvry S, Petit J. Effect of variable normal force and frequency on fretting wear response of Ti – 6Al – 4V contact. Wear 2011;271:1535–1542. 10.1016/j.wear.2011.01.060.

[18] Li J, Ma M, Lu YH, Xin L. Evolution of wear damage in Inconel 600 alloy due to fretting against type 304 stainless steel. Wear 2016;346–347:15–21. 10.1016/j.wear.2015.10.011.

[19] Nurmi V, Hintikka J, Juoksukangas J, Honkanen M, Vippola M, Lehtovaara A, et al. The formation and characterization of fretting-induced degradation layers using quenched and tempered steel. Tribol Int 2018;131:258–267. https://doi.org/10.1016/j.triboint.2018.09.012.

[20] Sauger E, Fouvry S, Ponsonnet L, Kapsa PP, Martin JM, Vincent L. Tribologically transformed structure in fretting. Wear 2000;245:39–52. 10.1016/S0043-1648(00)00464-6.

[21] Everitt NM, Ding J, Bandak G, Shipway PH, Leen SB, Williams EJ. Characterisation of fretting-induced wear debris for Ti-6Al-4 V. Wear 2009;267:283–291. 10.1016/j.wear.2008.12.032.

[22] Juoksukangas J, Lehtovaara A, Mäntylä A. Experimental and numerical investigation of fretting fatigue behavior in bolted joints. Tribol Int 2016;103:440–448. https://doi.org/10.1016/j.triboint.2016.07.021.

[23] Waterhouse RB. Fretting fatigue. London: Applied Science Publishers; 1981.

[24] Juoksukangas J, Nurmi V, Hintikka J, Vippola M, Lehtovaara A, Mäntylä A, et al. Characterization of cracks formed in large flat-on-flat fretting contact. Int J Fatigue 2019;124:361–370. 10.1016/j.ijfatigue.2019.03.004.

[25] Hintikka J, Mäntylä A, Vaara J, Frondelius T, Lehtovaara A. Stable and unstable friction in fretting contacts. Tribol Int 2019;131:73–82. https://doi.org/10.1016/j.triboint.2018.10.014.

[26] Mutoh Y, Tanaka K. Fretting fatigue in several steels and a cast iron. Wear 1988;125:175–191.

[27] Xin L, Lu Y, Shoji T. The role of material transfer in fretting wear behavior and mechanism of Alloy 690TT mated with Type 304 stainless steel. Mater Charact 2017;130:250–259. 10.1016/j.matchar.2017.06.020.